

Studies on the mechanisms of powerful terahertz radiations from laser plasmas

(Invited Paper)

Weimin Wang (王伟民)^{1*}, Zhengming Sheng (盛政明)^{1,2**}, Yutong Li (李玉同)¹, Liming Chen (陈黎明)¹, Quanli Dong (董全力)¹, Xin Lu (鲁欣)¹, Jinglong Ma (马景龙)¹, and Jie Zhang (张杰)^{1,2}

¹Beijing National Laboratory of Condensed Matter Physics, Institute of Physics, Chinese Academy of Sciences, Beijing 100190, China

²Key Laboratory for Laser Plasmas (Ministry of Education), Department of Physics, Shanghai Jiao Tong University, Shanghai 200240, China

*Corresponding author: hbwwm1@iphy.ac.cn; **corresponding author: zmsheng@sjtu.edu.cn

Received July 5, 2011; accepted August 8, 2011; posted online October 25, 2011

A survey on the mechanisms of powerful terahertz (THz) radiation from laser plasmas is presented. Firstly, an analytical model is described, showing that a transverse net current formed in a plasma can be converted into THz radiations at the plasma oscillation frequency. This theory is applied to explain THz generation in a gas driven by two-color laser pulses. It is also applied to THz generation in a tenuous plasma driven by a chirped laser pulse, a few-cycle laser pulse, a DC/AC bias electric field. These are well verified by particle-in-cell simulations, demonstrating that THz radiations produced in these approaches are nearly single-cycles and linear polarized. In the chirped laser scheme and the few-cycle laser scheme, THz radiations with the peak field strength of tens of MV/cm and the peak power of gigawatt can be achieved with the incident laser intensity less than 10^{17} W/cm².

OCIS codes: 350.5610, 300.6495, 260.5210, 350.5400, 320.7120.

doi: 10.3788/COL201109.110002.

1. Introduction

Terahertz (THz) waves with the field strength up to MV/cm or beyond are demanded for broad applications, such as nonlinear THz spectroscopy, THz nonlinear physics in condensed matters and semiconductors, nonperturbative THz electro-optics, etc.^[1,2]. Such THz waves are usually obtained from accelerator-based sources, which are still limited by the bandwidth, waveform, and the availability to most users. Therefore, table-top powerful THz sources^[3–9] based on laser-plasma interactions or laser-gas interactions have been attracting significant attention recently. For example, strong THz radiations can be produced from the laser wakefield in inhomogeneous plasmas by linear mode conversion^[4] or from the transition radiation at plasma-vacuum boundaries using ultrashort electron bunches produced from laser wakefield acceleration^[8]. The two-color laser scheme has been most intensively investigated in the last 10 years. Using this scheme, a linearly-polarized THz radiation of a few of hundred kV/cm has been demonstrated experimentally^[9–14], which is the strongest THz radiation driven by lasers. However, this scheme does not display a favorable scaling of the THz intensity with the laser intensity when the latter is high enough^[15]. An air plasma channel driven by a short intense laser pulse was also experimentally shown to be capable of emitting a radically polarized THz radiation by Cherenkov-like emission^[16,17]. Such a THz radiation is weaker than that produced from the two-color laser scheme. The THz radiation can be strengthened considerably provided that a DC bias field is applied to the air plasma channel^[18]. In this case, the THz radiation

becomes linearly polarized along the bias field direction and the THz amplitude is determined by the bias field strength. The amplitude of such a THz radiation is limited by the bias field amplitude available^[19], generally smaller than a few tens of kV/cm. This THz radiation can be enhanced to some degree when an AC/DC bias is applied^[19].

The THz generation mechanism of both the two-color laser scheme and the DC/AC bias field scheme can be explained as that of a net current being formed in a plasma and then converted into THz radiations at the plasma oscillation frequency through plasma dynamics^[15,19]. In the two-color laser scheme, the second harmonic light breaks the symmetry of the fundamental light ionization of gas^[14,15,20] and forms a transverse net current in the gas plasma. In the DC/AC bias field scheme, a net current is formed along the bias direction. According to the THz generation mechanism, two schemes are proposed to achieve THz radiations with the field strength meeting the requirements of the applications^[1,2]. The first scheme uses a laser pulse of a few-cycle duration to produce a MV/cm–GV/cm THz radiation, because single-cycle laser pulses with the carrier-envelope (CE) phases controlled are available^[21,22]. The waveforms of such lasers can become highly asymmetric at certain CE phases. An asymmetric laser pulse can induce a strong net transverse current as it passes through a plasma. The second scheme is to take a chirped laser pulse. A net current can be excited efficiently because the half-cycle laser field is asymmetric with the following half-cycle field. In the two schemes, the produced THz radiation amplitude scales linearly with the incident laser amplitude.

The outline of the paper is as follows. In section 2, the

mechanism of THz radiation generation from a transverse net current in a plasma is described by a theoretic model. In sections 3–6, the theory is applied to four examples in which the net currents are formed by two-color laser pulses in the gas ionization process, by a few-cycle laser pulse in a plasma, by a chirped laser pulse in a plasma, and by applying a bias DC/AC electric field in a plasma, respectively. Finally, the paper concludes in section 7.

2. Theoretical model

There are a few of schemes to generate a transverse net current in a plasma and then the net current is converted into THz radiations, e.g., the well-known two-color laser scheme^[9,15], the few-cycle laser scheme^[23], the chirped laser scheme^[15], and the bias electric field scheme^[18,19]. In this section, we assume that a transverse net current has been formed in a plasma and analyze how the current is converted into a THz radiation. The analytic results will then be applied to the four schemes mentioned above in the next four sections.

A. THz radiations from net transverse currents in plasmas

The generation of the THz radiation is analyzed by a theoretical model in one-dimensional (1D) approximation. Assume that there is a quasi-static net current $J_{y0} = -en_e v_{y0}$ along the y -direction in a plasma, where e is the electron charge, n_e is the plasma electron density, and v_{y0} are the velocities. This net current can be converted into a THz radiation^[15,19,23] by plasma dynamics. The physical mechanism is described as follows. Once a temporal or spacial fluctuation (a spacial fluctuation can cause a temporal one) appears in the quasi-static net current (e.g., a fluctuation in the electron velocities or the plasma density), an EM (or THz) radiation is formed with the electric field E_{THz} along the y direction, in terms of the wave equation

$$\left(\frac{\partial^2}{\partial x^2} - \frac{\partial^2}{c^2 \partial t^2}\right) E_{\text{THz}} = \frac{4\pi}{c^2} \frac{\partial J_y}{\partial t}. \quad (1)$$

In turn, E_{THz} acts on the plasma electrons and then the electron velocities v_{y0} become $v_y = v_{y0} - \int_{\xi_p}^{\xi} e E_{\text{THz}} / m_e d\xi$, which perturbs the net current further. The perturbation of the net current reinforces E_{THz} again. Due to this feed-back loop, the net current is converted into the THz radiation. For convenience, we use the vector potential A_{THz} of E_{THz} is used to express the electron velocities as

$$v_y = \frac{e A_{\text{THz}}}{m_e c} + v_{y0}, \quad (2)$$

and the wave equation as

$$\left(\frac{\partial^2}{\partial x^2} - \frac{\partial^2}{c^2 \partial t^2} - \frac{\omega_p^2}{c^2}\right) A_{\text{THz}} = \frac{4\pi e n_e v_{y0}}{c}, \quad (3)$$

where $\omega_p = \sqrt{4\pi e^2 n_e / m_e}$ is the plasma oscillation frequency and J_y has been replaced by $-en_e v_y$ in the wave equation. Here, we neglect the Lorentz forces of the electrons by the THz magnetic field, because the THz

radiation is not relativistic.

B. Frequencies and waveforms of the THz radiations

The solution of Eq. (3) in an infinite plasma was obtained in Ref. [19] and the properties of the solution in a semi-infinite plasma were discussed in Ref. [15]. In the two cases, the THz radiation is shown to have the frequency of ω_p , which is easy to understand from the three terms of Eq. (3) on the left hand. If there is a vacuum-plasma boundary, the THz radiation source in the plasma will propagate into the vacuum via the boundary. Considering a vacuum-plasma boundary, the exact solution of Eq. (3) is difficult to derive. However, it can be predicted that the THz radiation in the vacuum has the central frequency of ω_p and a near single-cycle waveform. This is because the THz radiation source at ω_p can penetrate into the vacuum only through the skin effect. The head of the THz radiation into the vacuum is the strongest, which comes from the THz source closest to the vacuum-plasma boundary. The sequent part of the THz radiation in the vacuum becomes weaker, which comes from the THz source farther from the vacuum-plasma boundary. Due to the skin effect, the THz radiation source only within the spacial range of about one λ_p or λ_T near the vacuum-plasma boundary can penetrate into the vacuum efficiently. Thus, the first cycle of the THz radiation in the vacuum is much stronger than the sequent part. Such a waveform and the central frequency of the THz radiation in the vacuum have been shown by the particle-in-cell (PIC) simulations in Refs. [15] and [19]. These will also be seen either in the following PIC simulations or the solution presented below under some approximations.

C. A solution under the approximation of an infinitesimal size plasma

Equation (3) is solved to obtain the THz radiation waveform in the vacuum. From Eq. (3) one can get

$$4 \frac{\partial^2}{\partial \xi \partial \psi} A_{\text{THz}} + \omega_p^2 A_{\text{THz}} + 4\pi e c n_e v_{y0} = 0, \quad (4)$$

by replacing t and x with $\xi = t - x/c$ and $\psi = t + x/c$. One can solve Eq. (4) by the Laplace transform method and obtain the solution:

$$A_{\text{THz}} = \frac{m_e c v_{y0}}{e} \left[J_0(\omega_p \sqrt{\xi \psi}) - 1 \right], \quad (5)$$

where J_0 is the order-order Bessel function. Here, we neglect the change of n_e with time and space. The approximation of an infinitesimal size plasma is taken to make sure that A_{THz} at $\xi > 0$ and $\psi > 0$ exists at the same time and space. Without this approximation, the analytical expression of the THz waveform is difficult to give (also see Ref. [15]).

Equation (5) presents the THz vector potential in the plasma. At the left vacuum-plasma boundary the THz vector potential is $A_{\text{THz}}(t, x=0) = \frac{m_e c v_{y0}}{e} \left[J_0(\omega_p t) - 1 \right]$. Therefore, in the left vacuum the THz vector potential is $A_{\text{THz}} = \frac{m_e c v_{y0}}{e} \{ J_0[\omega_p(t + x/c)] - 1 \}$. Then the THz electric field in the left vacuum is

$$E_{\text{THz}} = \frac{m_e \omega_p v_{y0}}{e} J_1 \left[\omega_p \left(t + \frac{x}{c} \right) \right], \quad (6)$$

where J_1 is the first-order Bessel function. Equation (6) shows that the THz radiation has the central frequency of ω_p and a near single-cycle waveform. The THz field in the right vacuum can be given by $E_{\text{THz}} = \frac{m_e \omega_p v_{y0}}{e} J_1 \left[\omega_p \left(t - \frac{x}{c} \right) \right]$ in the same way.

D Amplitude scaling of the THz radiations

From Eq. (3), one can achieve the scaling of the amplitude of the THz radiation with incident laser parameters. Considering v_{y0} is a constant with respect to t and x , one can obtain

$$A_{\text{THz}} \propto v_{y0}. \quad (7)$$

In the following sections, Eq. (7) will be applied to different cases to determine the dependence of the THz amplitude on laser parameters.

3. THz radiation driven by two-color laser pulses in a gas

Firstly, THz emission from a gas is investigated. Interaction of ultrashort laser pulses with tenuous gases includes the laser field ionization of gases and the interaction of the laser pulses with formed plasmas. For the j th electron, it follows the equation of motion given by

$$v_{y,j}(x, t) = \frac{e}{m_e c} [\mathbf{A}_L(x, t) - \mathbf{A}_L(x_{j0}, t_{j0})], \quad (8)$$

where \mathbf{A}_L is laser vector potential polarized along the y direction, and we set that the j th electron is born at place x_{j0} and time t_{j0} . We assume that the initial velocity of all newly born free electrons is zero. After the laser pulse passes through the electron, it gains a net velocity

$$v_{y,j} = -\frac{e}{m_e c} \mathbf{A}_L(x_{j0}, t_{j0}), \quad (9)$$

which is determined by the born place and time $t - x/c$. The average velocity of electrons at x and t is given by

$$v_{y0} = \sum_{j=1}^N v_{y,j} / N = -\frac{e}{m_e c} \langle \mathbf{A}_L(x_0, t_0) \rangle, \quad (10)$$

where $\langle \mathbf{A}_L(x_0, t_0) \rangle = \sum_{j=1}^N \mathbf{A}_L(x_{j0}, t_{j0}) / N$, N is the total electron number at x and t , and $\langle \mathbf{A}_L(x_0, t_0) \rangle$ should be a function of $x - ct$. Assume the ionization stops at x_f where laser pulses have left or gas atoms have been ionized completely. Then all $\langle \mathbf{A}_L(x_0, t_0) \rangle$ at $x < x_f$ should be statistically the same and quasi-static transverse currents are formed in the wake of the laser pulse.

The above analysis is applicable for gas targets irradiated by either one-color or two-color laser pulses. When one-color lasers are incident, the THz pulses will be produced relatively inefficiently. When two-color lasers are incident, the symmetry of positive and negative half-cycle of the fundamental wave is broken^[9,15]. The two-color-laser ionization causes net currents in the same direction in every cycle and can thus emit THz pulses more efficiently than one-color lasers (this holds only when the lasers are not intense^[25]). When the target is a fully ionized plasma slab, either one-color or

two-color waves are adopted, the net current is null, i.e., $v_{y0} = 0$, and no THz pulses can be generated.

To check the above results, 1D PIC simulations are used. In our PIC code, the field ionization of gases is included with tunneling ionization rates calculated by the ADK formula^[24]. For simplicity, only hydrogen gas (H_2) is used, which generates one kind of plasma density only. A slab target with the gas density $n_{\text{gas}} = 1.25 \times 10^{-5} n_c$ and the length $L_{\text{gas}} = 200 \lambda_0$ is used starting from $x = 500 \lambda_0$, where $n_c = m_e \omega_0^2 / 4\pi e^2$ is the critical density and $\omega_0 = 2\pi / T_0$ is the laser frequency. A laser pulse is incident along the $+x$ direction with the vector potential $\mathbf{A}_L = \hat{\mathbf{e}}_y a_L$, where $a_L = \sin^2(\pi \xi / \tau_0) \cdot [a_1 \cos(k_0 \xi) + a_2 \cos(2k_0 \xi + \theta)]$, $k_0 = \omega_0 / c$, τ_0 is pulse duration, a_1 and a_2 are normalized amplitudes for the fundamental and the second-harmonic waves, respectively, and θ is their relative phase. In the following simulations $\tau_0 = 20 \lambda_0$, $a_2 = a_1 / 2$, and $\theta = \pi / 2$.

The temporal and spatial distribution of THz emission is shown in Fig. 1(a). There are two THz pulses, one going along the $+x$ direction and the other along the $-x$ direction. These THz pulses penetrate into the vacuum and have a waveform with the first cycle being the strongest. This can be seen more clearly in Fig. 1(b), which shows the temporal evolution of THz pulses observed at $20 \lambda_0$ in front of the left gas-vacuum boundary. Their corresponding spectra are plotted in Fig. 1(c). One can see that the THz pulses have frequencies of $0.003 \omega_0$ (1 THz), $0.005 \omega_0$, and $0.01 \omega_0$, which are equal to their individual ω_p . Note that there is the 0-frequency component because of the asymmetry of the positive and negative peaks of the THz pulse. These are consistent with the previous analysis.

4. THz radiation driven by a chirped laser pulse in a plasma

Reference [15] shows that the THz intensity does not scale monotonically with the laser intensity in the two-color laser scheme due to the difficultly controlled gas

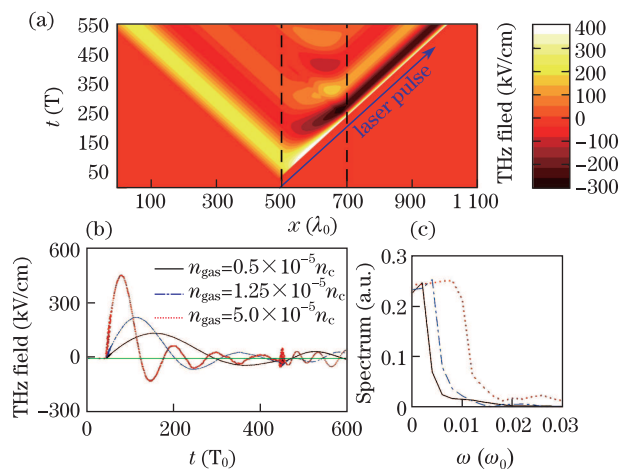


Fig. 1. (a) Temporal and spatial distribution of THz pulses from a H_2 gas target with the density $n_{\text{gas}} = 1.25 \times 10^{-5} n_c$. Waveforms (b) and spectra (c) of THz pulses from H_2 targets with different initial gas densities. A two-color laser with $a_1 = 0.06$ is taken. This figure can also be seen in Ref. [15].

ionization. We propose using a single chirped laser pulse irradiating on a plasma target, so that electrons can get net acceleration in the transverse direction during each laser period. If the chirping value sign of the laser is fixed, then the net acceleration of electrons will be found in the same direction in all laser periods, which can cause very strong net currents. To demonstrate the scheme mentioned above in a simple way, we take the chirped pulse electric field $\mathbf{E}_L = \hat{\mathbf{e}}_y \varepsilon_L$ with

$$\varepsilon_L = a_0 \sin[k_0 \xi(1 + C\xi)] \sin(\pi\xi/L_t^C), \quad (11)$$

where the pulse duration $L_t^C = (\sqrt{1 + 4CL_t^0} - 1)/2C$ for the chirping parameter C and L_t^0 is the pulse duration at $C = 0$. For positively chirped pulses $C > 0$, $L_t^C < L_t^0$ and for negatively-chirped pulses $C < 0$, $L_t^C > L_t^0$, when the total period number of laser pulses stays the same at any given C . Taking such chirped pulses, one can easily calculate the net transverse net velocity v_{y0} . For example, when $C = 1.0$ and -0.024 , there are $v_{y0} = -0.0115a_0 2\pi e/m_e \omega_0$ and $0.0413a_0 2\pi e/m_e \omega_0$, respectively. According to Eq. (6), one can obtain

$$E_{\text{THz}}(C = 1.0) = \frac{-0.07a_0 \omega_p}{\omega_0} J_1 \left[\omega_p \left(t + \frac{x}{c} \right) \right], \quad (12)$$

and

$$E_{\text{THz}}(C = -0.024) = \frac{0.26a_0 \omega_p}{\omega_0} J_1 \left[\omega_p \left(t + \frac{x}{c} \right) \right]. \quad (13)$$

PIC simulations are used to test the analysis above. We fix the C , change the pulse amplitude, and obtain the THz amplitude as a function of a_0 , which is shown in Fig. 2. The THz pulse amplitude is shown to increase linearly with a_0 for both positive and negative chirped pulses. The ratio of slopes $[\partial E_{\text{THz}}/\partial a_0]_{C=-0.024}/[\partial E_{\text{THz}}/\partial a_0]_{C=1.0} = -3.59$ is exactly confirmed by Fig. 2. According to the simulations, when $a_0 = 0.067$ (6.1×10^{15} W/cm²) and $C = -0.024$, the THz amplitude is 1 MV/cm. According to Eq. (13), the THz amplitude is 1.6 MV/cm, which is in approximate agreement with the simulations.

5. THz radiation driven by a few-cycle laser pulse in a plasma

A transverse net current can also be produced in a plasma if a few-cycle laser pulse is taken through controlling its CE phase^[24]. A laser pulse with the linear polarization is taken along the y direction propagating in the $+x$ direction. The laser electric field has the form of $E_y = E_0 \exp(-\xi^2/\tau_0^2) \sin(\omega_0 \xi + \theta)$, where $2\sqrt{\ln 2}\tau_0$ is the FWHM duration, θ is the CE phase, $\xi = t - x/c$, and c is the speed of light in the vacuum. The laser pulse illuminates upon a tenuous plasma. The plasma electrons move under the laser electric field with velocities $\int_{-\infty}^{\xi} -eE_y/m_e d\xi$. After the laser pulse passes through the electrons, they gain the velocities $v_{y0} = \int_{-\infty}^{\xi_p} -eE_y/m_e d\xi \rightarrow \int_{-\infty}^{+\infty} -eE_y/m_e d\xi$. One can obtain

$$v_{y0} = -\frac{e\sqrt{\pi}}{m_e} E_0 \tau_0 \exp\left(-\frac{\omega_0^2 \tau_0^2}{4}\right) \sin(\theta). \quad (14)$$

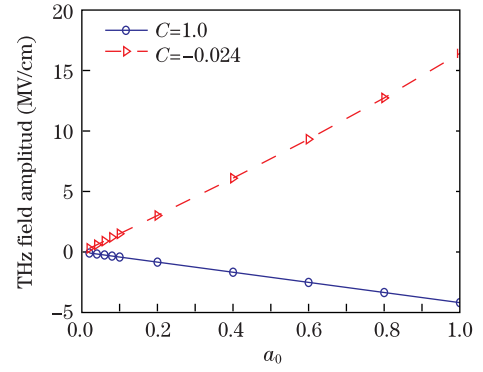


Fig. 2. THz pulse amplitude as a function of the chirped laser amplitude for two different chirping parameters, where the electron density is $2.5 \times 10^{-5} n_c$ and a plasma target is taken. This figure can also be seen in Ref. [15].

We take such ξ_p that $E_y(\xi_p) \rightarrow E_y(+\infty) \rightarrow 0$. This can be satisfied if ξ_p is taken as a few of τ_0 .

From Eqs. (14) and (7), one can achieve the scaling of the amplitude of the THz radiation as

$$A_{\text{THz}} \propto E_0 \tau_0 \exp\left(-\frac{\omega_0^2 \tau_0^2}{4}\right) \sin(\theta). \quad (15)$$

In terms of Eq. (15), the THz amplitude enhances exponentially with the decrease of τ_0 and it reaches the maximum when $\tau_0 = \sqrt{2}/\omega_0$. For example, as the laser FWHM duration $2\sqrt{\ln 2}\tau_0$ changes from 1.5 cycles to 1.0 and 0.5 cycles, the THz amplitude increases by 57 and 412 times, respectively. While τ_0 is large, $\tau_0 \exp(-\omega_0^2 \tau_0^2/4)$ is quite small and nearly no THz radiation can be produced, as is usually encountered. The CE phase is also a key parameter and the THz amplitude is proportional to $\sin(\theta)$. Moreover, the THz amplitude scales linearly with the laser amplitude E_0 .

In addition, from Eqs. (6) and (14) one can obtain

$$E_{\text{THz}} = -\sqrt{\pi} \omega_p E_0 \tau_0 \sin(\theta) \exp\left(-\frac{\omega_0^2 \tau_0^2}{4}\right) J_1 \left[\omega_p \left(t + \frac{x}{c} \right) \right]. \quad (16)$$

These 1D results are expected to be valid because the laser spot size is much larger than its wavelength.

Then Eqs. (15) and (16) are then checked through 2D PIC simulations. A 1- μm -wavelength laser, with the electric field $E_y = E_0 \exp(-\xi^2/\tau_0^2 - y^2/r_0^2) \sin(\omega_0 \xi + \theta)$, propagates along the $+x$ direction. A plasma slab is distributed between $x = 180 \mu\text{m}$ and $x = 280 \mu\text{m}$. It has a uniform density profile with the electron density $n_e = 1.2 \times 10^{18} \text{ cm}^{-3}$ (or $\omega_p/2\pi = 10$ THz). The test standard simulation parameters are the laser FWHM duration 3.3 fs or one laser cycle, the CE phase $\theta = 90^\circ$, the laser intensity $10^{17} \text{ W} \cdot \text{cm}^{-2}$, and the spot radius $r_0 = 20 \mu\text{m}$. The following simulations are performed either with the standard parameters or with one of these parameters changed.

Figure 3 shows the spatial distributions of the produced THz radiation propagating along the $-x$ direction in the vacuum on the left of the plasma. The left column (a) in Fig. 3 is the simulation results with the standard parameters. One can see that the transversely

spatial distribution of the THz field at $t = 100$ fs follows $\exp(-y^2/r_0^2)$. Its amplitude is about 16 MV/cm at $t = 100$ fs. As it propagates leftwards, its wavefront spreads outside and it attenuates gradually. In addition, the single-cycle waveform of the THz radiation can be observed clearly. When the laser FWHM duration is increased to 1.25 cycles (or 4.2 fs), the spatial distributions of the THz radiation are shown in the right column (b) in Fig. 3. The distributions of the THz radiation are similar to those shown in Fig. 1(a). However, its amplitude at $t = 100$ fs is about 3 MV/cm, which is 4.3 times smaller than that in Fig. 3(a). This agrees with the expectation of Eq. (15).

Further simulations with different laser FWHM durations within 0.5 to 4 cycles are performed. The temporal waveforms of the THz radiation obtained from four typical simulations are shown in Fig. 4(a), where these waveforms are observed at $y = 0$ and $x = 162 \mu\text{m}$ (or $18 \mu\text{m}$ away from the left boundary of the plasma). These THz waves have central frequencies around $\omega_p/2\pi = 10$ THz and near single-cycle profiles. We obtain the THz

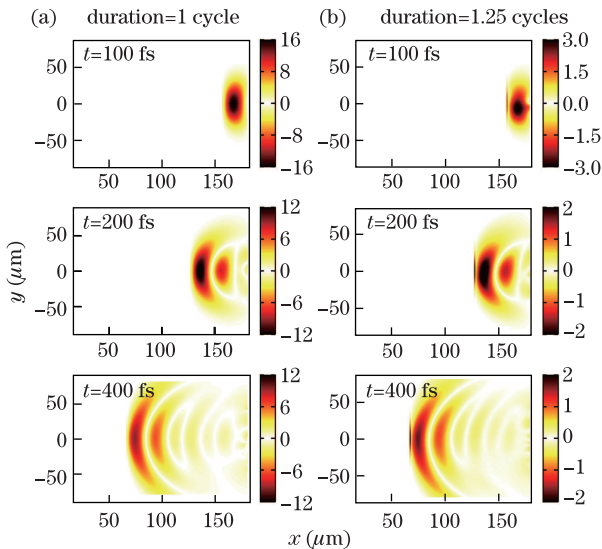


Fig. 3. (Color online) Snapshots of the spatial distributions of THz electric fields with the unit of MV/cm. (a) The simulation results with the standard parameters. (b) The simulation results with the standard parameters, except for when the laser FWHM duration of 1.25 cycles is used.

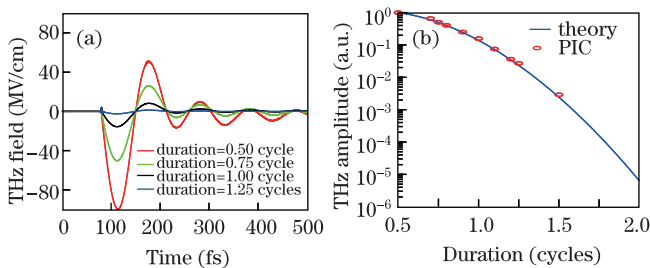


Fig. 4. (Color online) (a) The temporal waveforms of the THz electric fields at $x = 162 \mu\text{m}$ and $y = 0$ for different laser FWHM durations. (b) The THz amplitude as a function of the laser FWHM duration, where the amplitude is normalized by that with the laser FWHM duration of 0.5 cycle. The circles are the PIC results and the solid curve is given by Eq. (3) with $\theta = 90^\circ$.

amplitude from such temporal waveforms and display the THz amplitude as a function of the laser FWHM duration by the circles in Fig. 4(b). In this figure, the THz amplitude is normalized by that with the laser FWHM duration of 0.5 cycle. The solid curve is given by Eq. (15) with $\theta = 90^\circ$. One can see that the PIC results are in good agreement with the theoretic results. In particular, with the decrease of the laser FWHM duration from 1.5 cycles to 0.5 cycle, the THz amplitude enhances by about three orders of magnitude. When the duration is larger than two cycles, the THz radiation observed becomes weak to the numerical noise level.

The laser CE phase θ between 0° and 180° is then changed. The temporal waveforms of the THz radiation are shown in Fig. 5(a). The THz amplitude as a function of the CE phase is displayed by the circles in Fig. 5(b). The dependence of the THz amplitude on the CE phase follows the sine function accurately, which is consistent with Eq. (15). Particularly, when the CE phase is 90° , the THz radiation is the strongest. This provides a method to measure the CE phase of an ultrashort laser by the intensity of the THz or electromagnetic radiation.

Next, we change the laser intensity within $10^{15} - 10^{18} \text{ W} \cdot \text{cm}^{-2}$ is changed. Figure 6(a) shows the temporal waveforms of the THz radiation at different laser intensities and Fig. 6(b) is the THz intensity versus the laser intensity. One can see that the THz intensity scales linearly with the laser intensity, which accords with Eq. (15). The laser at even $10^{15} \text{ W} \cdot \text{cm}^{-2}$ is also observed to produce $3.3 \times 10^9 \text{ W} \cdot \text{cm}^{-2}$ THz radiation (or the amplitude of about 1.6 MV/cm). According to Fig. 6(a), one can calculate the peak powers of the THz radiations because their transversely spatial distributions follow $\exp(-y^2/r_0^2)$ approximately. One can predict that the generation of the 1 GW THz radiation needs the half-cycle laser of 8 TW or the single-cycle laser of 300 TW, which is independent of the laser intensity.

In addition, all of the above simulation results are in approximate agreement with Eq. (16). For example, with the test standard simulation parameters (the laser FWHM duration is one laser cycle and the laser intensity is $10^{17} \text{ W} \cdot \text{cm}^{-2}$), the THz amplitude is 31 MV/cm, which is not much different from the 16 MV/cm value obtained from the simulations of Fig. 3. Actually, the THz amplitude is 21 MV/cm for our other simulation with a plane laser. The THz waveforms in Figs. 4–6 can also be approximately described by Eq. (16).

6. THz radiation driven by a DC/AC bias field in a plasma

A straightforward scheme^[19] is then proposed wherein a bias electric field is applied on a plasma and then a static net current is formed. We take a bias electric field with an arbitrary frequency, $\mathbf{E}_{\text{bias}} = \hat{e}_y E_0 \cos(\omega t)$. Set the vector potential of the plasma response field as \mathbf{A} , then the equation of motion for electrons is given by $m_e \partial \mathbf{v} / \partial t = -e(\mathbf{E}_{\text{bias}} - \partial \mathbf{A} / c \partial t)$, where the bias field is assumed to be much weaker than the relativistic correction and the Lorentz force is neglected. Then one can derive velocities of electrons as

$$v_y = [-eE_0 \sin(\omega t) / m_e \omega + eA / m_e c], \quad (17)$$

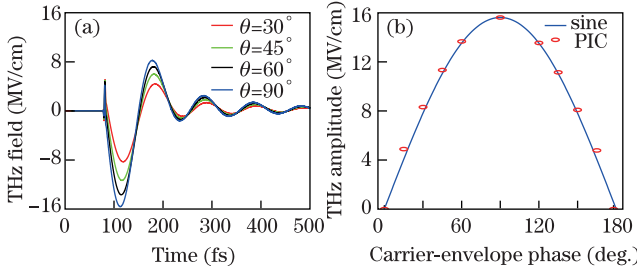


Fig. 5. (Color online) The temporal waveforms of the THz electric fields at $x = 162 \mu\text{m}$ and $y = 0$ for different laser CE phases. (b) The THz amplitude as a function of the laser CE phase. The circles are the PIC results and the solid curve is the sine function of the laser CE phase.

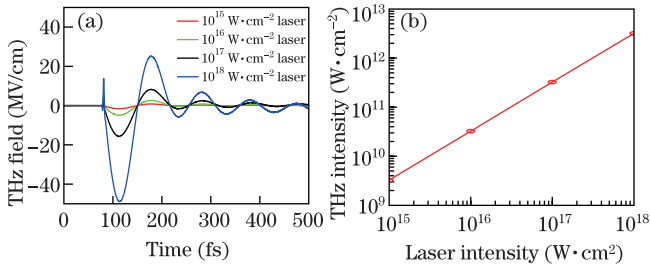


Fig. 6. (Color online) (a) The temporal waveforms of the THz electric fields at $x = 162 \mu\text{m}$ and $y = 0$ for different laser intensities. (b) The THz intensity as a function of the laser intensity.

where we have assumed the initial electron velocity and fields are assumed to have vanished before the bias is triggered. Neglecting the motion of the plasma ions, we calculate the current density $J_y = -n_e e v$, insert it into the wave equation, and obtain

$$\left(c^2 \frac{\partial^2}{\partial x^2} - \frac{\partial^2}{\partial t^2} - \omega_p^2 \right) A = -\frac{c \omega_p^2}{\omega} E_0 \sin(\omega t). \quad (18)$$

If the bias and the plasma are distributed uniformly in space, Eq. (17) can be simplified into

$$\frac{\partial^2 A}{\partial t^2} + \omega_p^2 A = (\omega_p^2 c / \omega) E_0 \sin(\omega t). \quad (19)$$

From Eq. (18) the electric field of the plasma response is given by

$$E_y = \begin{cases} \frac{\omega_p^2 E_0}{\omega_p^2 - \omega^2} [\cos(\omega_p t) - \cos(\omega t)], & \omega \neq \omega_p \\ -\frac{\omega_p t E_0}{2} \sin(\omega_p t), & \omega = \omega_p \end{cases}. \quad (20)$$

The electric field clearly has two components with the frequencies of ω and ω_p . For a DC bias, i.e., $\omega = 0$, $E_y = E_0 [\cos(\omega_p t) - 1]$, which includes both DC and ω_p 's components. For $\omega \in (0, \sqrt{2}\omega_p)$ the EM radiation is strengthened, compared with the case of a DC bias. In particular, when ω approaches to ω_p , a resonance appears and E_y is strengthened significantly.

For a plasma slab with a finite size in the x direction, the electric oscillation in the plasma can be converted partially into EM radiation along the $\pm x$ direction from the plasma to the vacuum. The frequency of the radiation field is the same with the electric oscillation in the

plasma. The radiation amplitude is also proportional to E_0 . In particular, for a DC bias pump, one can easily obtain the solution of Eq. (15)

$$E_{\text{THz}} = E_0 \left\{ J_0 \left[\omega_p \left(t \pm \frac{x}{c} \right) \right] - 1 \right\}. \quad (21)$$

Then 2D PIC simulations are run to verify the above results. Uniform plasmas with the electron density n_e within $10^{15} - 10^{19} \text{ cm}^{-3}$ and the thickness within $2\lambda_p$ are taken in the x direction, where $\lambda_p = 2\pi c / \omega_p$ is the plasma wavelength (e.g., $\lambda_p = 30 \mu\text{m}$ for the plasma with $n_e = 1.2 \times 10^{18} \text{ cm}^{-3}$). A DC/AC bias electric field with the amplitude E_0 within 10–1000 kV/cm and along the y direction is applied to the plasma.

In Fig. 7 we take a DC bias with $E_0 = 10 \text{ kV/cm}$. The spatial distribution of this EM radiation is plotted in Fig. 7(a). One can see that there are two planar EM waves propagating along the $\pm x$ direction from the plasma. The EM waves (E_y) oscillate at the center of $E_0 = 10 \text{ kV/cm}$ starting from $E_y = 0$.

The waveform properties of the EM waves can be seen more clearly in Fig. 8. Figures 8(a) and (c) are the

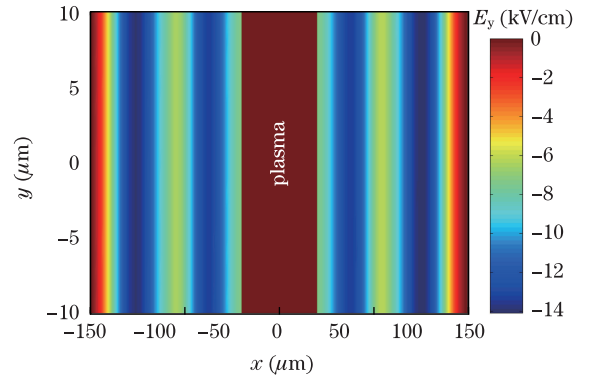


Fig. 7. (Color online) The spatial distribution of EM waves E_y at $t = 400 \text{ fs}$, where the plasma density is $1.2 \times 10^{18} \text{ cm}^{-3}$ and the DC bias field along the y -direction has the amplitude of 10 kV/cm . This figure can also be seen in Ref. [19].

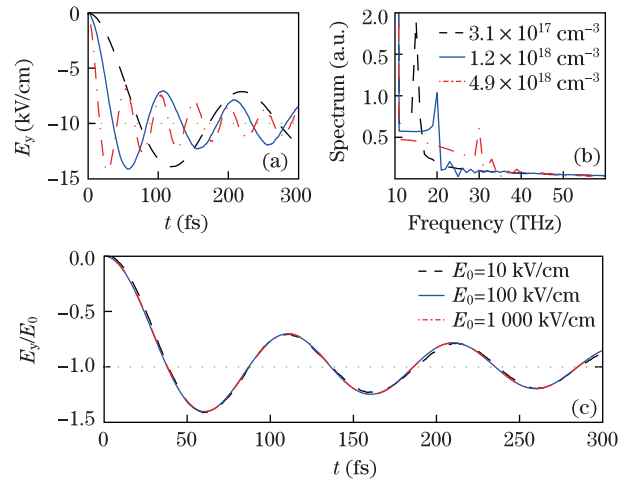


Fig. 8. (a) Waveforms of EM waves emitted from plasmas with different densities and (b) the corresponding spectra, where the DC bias field along the y -direction has the amplitude $E_0 = 10 \text{ kV/cm}$. (c) Waveforms of EM waves for different DC bias amplitudes, where the plasma density is $1.2 \times 10^{18} \text{ cm}^{-3}$. This figure can also be seen in Ref. [19].

temporal waveforms observed at 10 μm away from the left vacuum-plasma boundary. Three curves in Fig. 8(a) represent the cases for different plasma densities. Their corresponding spectra are plotted in Fig. 8(b), which shows that the EM waves have both a DC component and an ω_p 's component. Three curves in Fig. 8(c) display the EM waves for different bias field amplitudes E_0 , where they take the unit of the corresponding E_0 . One can see that these three curves nearly coincide, which indicates that the EM wave amplitude scales linearly with the bias amplitude exactly. As a result, a plasma can convert a dc bias field into EM radiation with the frequency and amplitude controlled by the plasma density and the bias amplitude, respectively. In addition, the waveform and the amplitude of the THz radiation accords with Eq. (21) very well.

7. Summary

In conclusion, theory and PIC simulations show that a net transient current produced in a plasma can be converted into THz radiations at the plasma oscillation frequency, which can explain THz generation mechanism in the two-color laser scheme. Under this theory, a few schemes to produce transverse net currents in tenuous plasma have been proposed, allowing for the generation of a powerful THz emission. These schemes include the chirped laser scheme, the few-cycle laser scheme, and the bias field scheme. The produced THz radiation amplitudes scale linearly with the laser amplitude or bias amplitude. In the chirped laser scheme and the few-cycle laser scheme, the asymmetric laser pulse is used to form a strong net current in the plasma and then produce powerful THz radiations. In the chirped laser scheme, one can take a large chirped value to obtain a high asymmetric laser pulse. In the few-cycle laser scheme, one can employ the CE phase of 90° to achieve an asymmetric laser pulse. In this case, a short laser pulse should be used because the THz radiation amplitude increases exponentially with the decrease of the laser duration. In particular, THz emission amplitude as large as tens of MV/cm is possible with the chirped laser scheme or the few-cycle laser scheme at the laser intensity of less than 10^{17} W/cm².

This work was supported in part by the National Natural Science Foundation of China (Nos. 11105217 and 10925421) and the National Basic Research Program of China (No. 2009GB105002).

References

1. M. S. Sherwin, C. A. Schmuttenmaer, and P. H. Bucksbaum, "DOE-NSF-NIH Workshop on Opportunities in THz Science" http://www.er.doe.gov/bes/reports/files/THz_rpt.pdf.
2. B. E. Cole, J. B. Williams, B. T. King, M. S. Sherwin, and C. R. Stanley, *Nature* **410**, 60 (2001).
3. H. Hamster, A. Sullivan, S. Gordon, W. White, and R. W. Falcone, *Phys. Rev. Lett.* **71**, 2725 (1993).
4. Z.-M. Sheng, K. Mima, J. Zhang, and H. Sanuki, *Phys. Rev. Lett.* **94**, 095003 (2005).
5. Z.-M. Sheng, K. Mima, and J. Zhang, *Phys. Plasmas* **12**, 123103 (2005).
6. Z.-M. Sheng, H.-C. Wu, K. Li, and J. Zhang, *Phys. Rev. E* **69**, 025401(R) (2004).
7. H.-C. Wu, Z.-M. Sheng, and J. Zhang, *Phys. Rev. E* **77**, 046405 (2008).
8. W. P. Leemans, C. G. R. Geddes, J. Faure, Cs. Toth, J. van Tilborg, C. B. Schroeder, E. Esarey, G. Fubiani, D. Auerbach, B. Marcellis, M. A. Carnahan, R. A. Kaindl, J. Byrd, and M. C. Martin, *Phys. Rev. Lett.* **91**, 074802 (2003).
9. D. J. Cook and R. M. Hochstrasser, *Opt. Lett.* **25**, 1210 (2000).
10. M. Kress, T. Löffler, S. Eden, M. Thomson, and H. G. Roskos, *Opt. Lett.* **29**, 1120 (2004).
11. T. Bartel, P. Gaal, K. Reimann, M. Woerner, and T. Elsaesser, *Opt. Lett.* **30**, 2805 (2005).
12. X. Xie, J. Dai, and X.-C. Zhang, *Phys. Rev. Lett.* **96**, 075005 (2006).
13. X.-Y. Peng, C. Li, M. Chen, T. Toncian, R. Jung, O. Willi, Y.-T. Li, W.-M. Wang, S.-J. Wang, F. Liu, A. Pukhov, Z.-M. Sheng, and J. Zhang, *Appl. Phys. Lett.* **94**, 101502 (2009).
14. K. Y. Kim, J. H. Glowina, A. J. Taylor, and G. Rodriguez, *Opt. Express* **15**, 4577 (2007).
15. W.-M. Wang, Z.-M. Sheng, H.-C. Wu, M. Chen, C. Li, J. Zhang, and K. Mima, *Opt. Express* **16**, 16999 (2008).
16. C. D'Amico, A. Houard, M. Franco, B. Prade, A. Mysyrowicz, A. Couairon, and V. T. Tikhonchuk, *Phys. Rev. Lett.* **98**, 235002 (2007).
17. Y. Liu, A. Houard, B. Prade, S. Akturk, A. Mysyrowicz, and V. T. Tikhonchuk, *Phys. Rev. Lett.* **99**, 135002 (2007).
18. A. Houard, Y. Liu, B. Prade, V. T. Tikhonchuk, and A. Mysyrowicz, *Phys. Rev. Lett.* **100**, 255006 (2008).
19. W.-M. Wang, Z.-M. Sheng, X.-G. Dong, H.-W. Du, Y.-T. Li, and J. Zhang, *J. Appl. Phys.* **107**, 023113 (2010).
20. H. C. Wu, J. Meyer-ter-Vehn, and Z. M. Sheng, *New J. Phys.* **10**, 043001 (2008).
21. A. L. Cavalieri, E. Goulielmakis, B. Horvath, W. Helml, M. Schultze, M. Fieb, V. Pervak, L. Veisz, V. S. Yakovlev, M. Uiberacker, A. Apolonski, F. Krausz, and R. Kienberger, *New J. Phys.* **9**, 242 (2007).
22. E. Goulielmakis, M. Schultze, M. Hofstetter, V. S. Yakovlev, J. Gagnon, M. Uiberacker, A. L. Aquila, E. M. Gullikson, D. T. Attwood, R. Kienberger, F. Krausz, and U. Kleineberg, *Science* **320**, 1614 (2008).
23. W.-M. Wang, S. Kawata, Z.-M. Sheng, Y.-T. Li, and J. Zhang, *Phys. Plasmas* **18**, 073108 (2011).
24. M. V. Ammosov, N. B. Delone, and V. P. Krainov, *Sov. Phys. JETP* **64**, 1191 (1986).
25. W.-M. Wang, S. Kawata, Z.-M. Sheng, Y.-T. Li, J. Zhang, L. M. Chen, L. J. Qian, and J. Zhang, *Opt. Lett.* **36**, 2608 (2011).